

Molecular Organization of Bovine Rod cGMP-Phosphodiesterase 6

Jacques F. Kameni Tcheudji¹, Luc Lebeau², Noëlle Virmaux³
Carmen G. Maftai⁴, Rick H. Cote⁴, Claire Lugnier¹ and Patrick Schultz^{5*}

¹*Pharmacologie et Physico-chimie des Interactions Cellulaires et Moléculaires UMR CNRS 7034, ULP, Faculté de Pharmacie, 74 route du Rhin, F-67401 Illkirch France*

²*Laboratoire de Synthèse Bioorganique, UMR CNRS 7514, ULP, 74 route du Rhin F-67401 Illkirch, France*

³*Centre de Neurochimie INSERM U 338, 5 rue Blaise Pascal F-67084, Strasbourg France*

⁴*Department of Biochemistry and Molecular Biology, University of New Hampshire 46 College Rd, Durham NH 03824-2617, USA*

⁵*Institut de Génétique et de Biologie Moléculaire et Cellulaire, ULP, CNRS, INSERM, 1 rue Laurent Fries BP163, F-67404 Illkirch France*

Phosphodiesterase 6 (PDE6), a multisubunit ($\alpha\beta\gamma_2\delta$) enzyme, plays a major role in visual function by hydrolysing cGMP in response to a light stimulus. Solubilized bovine rod PDE6 molecules depleted of their γ subunits were purified to homogeneity from bovine retinal rods and their molecular organization was investigated by electron microscopy. Image analysis of single particles revealed the three-dimensional dimeric arrangement of the purified $\alpha\beta\delta$ complex, and the internal organization of each catalytic subunit into three distinct domains at a resolution of 2.8 nm. The relative volume of each domain is consistent with sequence analysis and functional data, which suggest that these domains correspond to the catalytic and two GAF domains. This hypothesis was confirmed by immunolabelling experiments, which located the N-terminal part of the catalytic subunit where the major interaction between the two $\alpha\beta$ subunits was found to occur. The 3D molecular organization of human platelet PDE5 appears highly homologous to that of bovine rod PDE6, as predicted by similarities in their primary sequences. These observations describe the quaternary organization of the catalytic PDE6 $\alpha\beta$ complex, and place the catalytic and regulatory domains on a structural model.

© 2001 Academic Press

*Corresponding author

Keywords: PDE6; PDE5; electron microscopy; immunoelectron microscopy; image analysis

Introduction

The retinal rod outer segment cGMP phosphodiesterase (rod PDE6: EC 3.1.4.35) is the G-protein-activated effector enzyme for visual signal transduction. Rod PDE6 is a multisubunit complex, composed of two tightly bound catalytic subunits α (99 kDa)¹ and β (98 kDa)² in addition to two identical inhibitory γ subunits of 11 kDa.^{3,4} Rod

photoreceptors contain both a membrane-associated PDE and a soluble PDE, which co-purifies with a 17 kDa δ subunit.⁵ It is hypothesized that the δ subunit is responsible for the regulation of membrane attachment.⁶ The outer segment enzyme cascade is initiated when the visual pigment, rhodopsin, absorbs a photon. Each illuminated rhodopsin molecule activates many transducin molecules (a G-protein composed of α , β , and γ subunits) by catalysing the exchange of GDP for GTP. Once GTP is bound, the transducin T α -GTP subunit activates PDE6 by displacing the inhibitory γ subunits from the active site of the enzyme, thus allowing cGMP hydrolysis. The main function of the rod PDE6 is to rapidly reduce the steady-state

Abbreviations used: PDE6, cGMP phosphodiesterase 6; ROS, retinal rod outer segments; IC, immune complex.

E-mail address of corresponding author: pat@moorea.u-strasbg.fr

concentration of cGMP in response to the light stimulus. This decrease in cGMP concentration causes closure of cationic channels and generates a cell membrane hyperpolarization. This initial signal is transmitted *via* second-order retinal neurons to the optic nerve and to the brain.⁷

The primary structure of the four rod PDE6 subunits has been determined.^{1-3,6} The PDE6 α and β subunits show a high degree of homology (about 72%) and contain two functional domains: (1) a C-terminal region of about 275 amino acid residues that constitutes the catalytic domain for cyclic nucleotide hydrolysis, which is highly conserved for all known mammalian PDEs; (2) a regulatory domain in the N-terminal half of the sequence that contains two GAF domains⁸ that can bind cGMP with high affinity. The physiological significance of these non-catalytic cGMP binding sites is unclear, but it is known that they regulate the affinity of the γ subunits for the catalytic $\alpha\beta$ dimer.^{9,10}

The rod PDE6 complex is just one member of the sub-family of GAF domain-containing PDEs. Other members of this group are: cone PDE6, cGMP-stimulated PDE (PDE2), which hydrolyzes both cAMP and cGMP, cGMP-binding/cGMP-specific PDE (PDE5) and two newly discovered enzymes, PDE10 and PDE11 (for reviews, see Conti¹¹ and Francis *et al.*¹²). The rod photoreceptor PDE6 has several unique properties among the GAF-containing PDE family: the catalytic complex is a $\alpha\beta$ heterodimer, the catalytic α and β subunits anchored to the membrane by isoprenyl groups at their C terminus, enzyme activation results from binding of a heterotrimeric G-protein, the k_{cat} for cyclic nucleotide hydrolysis is $\sim 10^2$ -fold higher than other PDEs, and the catalytic activity is inhibited by the PDE γ subunit (reviewed by Artemyev *et al.*¹³). The PDE5 enzyme is most closely related to rod PDE6, based on amino acid sequence similarity,¹⁴ pharmacological properties^{15,16} and the presence of a γ -like protein that may associate with PDE5.^{17,18} However, the PDE5 homodimer exists in cells in a soluble form (although no homologous δ subunit has been reported), and its catalytic activity is not known to be regulated by G-protein activation.¹⁹

The structure of the C-terminal catalytic domain has been solved at atomic resolution for human recombinant PDE4B2B.²⁰ Moreover, the structure of the PDE5 GAF domain has been modelled, based on its homology with GAF domain-containing proteins.²¹ However, the molecular organization of the fully functional PDE complex is still not elucidated, which is a prerequisite to understanding how the catalytic and regulatory domains communicate and how the structure of the enzyme is modified upon transducin activation, cGMP binding, or γ subunit interaction. In the present work, we employed electron microscopy combined with numerical image analysis to describe the molecular structure of purified bovine retinal rod PDE6. This study revealed that the PDE6 α and β subunits each have an elongated shape and are

associated to form a pseudo 2-fold symmetry. Each subunit is divided into three distinct structural subdomains, whose sizes correspond to a large catalytic domain and two smaller cGMP-binding domains. This hypothesis was supported by immunolabelling of the α subunit N-terminal domain. The analysis of purified human blood platelet PDE5 showed that the overall structure is conserved between these two distinct PDE families. This study provides a structural model to further investigate the molecular mechanism and regulation of rod PDE6 activity during visual signal transduction.

Results

Purification, biochemical and pharmacological characterisation of bovine rod PDE6

Bovine PDE6 complexes were purified from retinal rod outer segments (ROS) as described.²² Highly purified PDE6 complexes were obtained by loading the soluble hypotonic extract of ROS onto a Sephadex HR-200 gel-filtration column. The PDE activity was tested throughout the fractionation, and the highest cGMP hydrolytic activity was found for fractions 29 to 31, which correspond to a relative molecular mass of about 200 kDa (Figure 1(a)). These fractions were pooled and concentrated. The kinetics of cGMP hydrolysis for purified PDE6 were determined and a K_m value of 27.7 μM and a V_{max} value of 42 $\mu\text{mol mg}^{-1} \text{min}^{-1}$ were obtained. The enzyme was potently inhibited by NH_2 -zaprinast and 1,3-dimethyl-6-(propoxy-5-methanesulfonylamidophenyl) pyrazolo[3,4d]-pyrimidin-4-(5H)-one (DMPPPO), two analogues of zaprinast (the conventional inhibitor of cGMP-specific PDEs) with respective IC_{50} values of 7 and 8 nM determined at 1 μM cGMP. These values were consistent with previously determined kinetic values.^{16,23,24}

The soluble hypotonic extract of ROS fractions and the purified PDE6 were analysed by SDS/8% (w/v) polyacrylamide gel electrophoresis (Figure 1(b), lanes 1 and 2, respectively). Both fractions contained a major double band at about 95 kDa, which corresponded to the PDE6 α and β subunits, as shown by a Western blot analysis using PDE6 α and β subunit-specific antibodies (Figure 1(b), lanes 3 and 4, respectively). The gel-filtration step resulted in the loss of the PDE6 γ subunit, as judged by a specific antibody showing that PDE6 γ is present in the hypotonic extract but absent after gel-filtration (Figure 1(b), lanes 5 and 6, respectively). Upon analysing all fractions of the gel-filtration eluant, the γ subunit could be detected in fractions 34 to 37, which corresponds to a molecular mass of 80-50 kDa (data not shown). The dissociation of this subunit from the PDE6 $\alpha\beta$ complex was reported to occur during gel-filtration and to be due to the interaction of the γ subunit with activated transducin α subunit present in the hypotonic extract.^{25,26} Antibodies raised

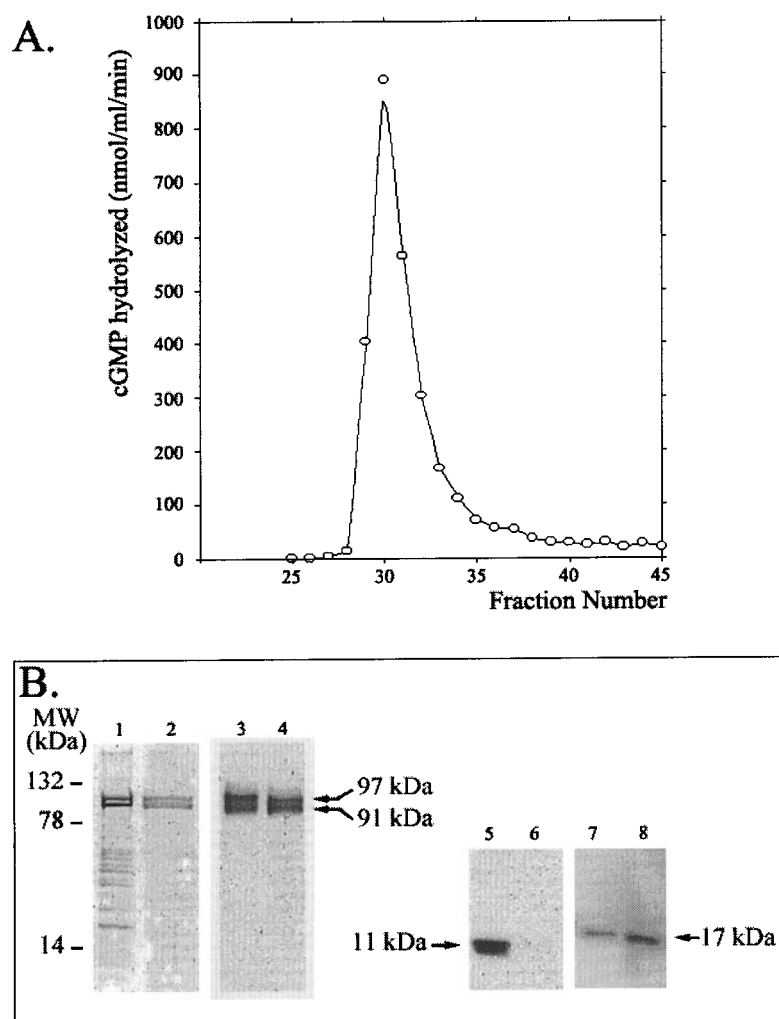


Figure 1. Purification and physico-chemical characterisation of retinal rod PDE6. (a) cGMP hydrolysis activity profile of retinal rod PDE6 isolated as described²² and purified by gel-filtration. (b) Coomassie-stained SDS-PAGE protein analysis of 150 ng of the soluble rod outer segment fraction (lane 1) and 30 ng of the gel-filtration peak fractions (lane 2). Western blot analysis using PDE6 α - and β -specific antibodies identifies a double band at ~ 95 kDa in the soluble rod outer segment fraction (lane 3) and in the gel-filtration peak fraction (lane 4) corresponding to the catalytic subunits. Western blot analysis using a PDE6 γ -specific antibody shows that this subunit, present in the soluble rod outer segment fraction (lane 5) is lost during gel-filtration (lane 6). Western blot analysis using a PDE6 δ -specific antibody identifies a band at 17 kDa in the soluble rod outer segment fraction (lane 7) and in the gel-filtration peak fraction (Lane 8) corresponding to the δ subunit. Molecular mass markers are indicated on the left of the lane 1.

against the δ subunit revealed a band at a molecular mass of 17 kDa, showing that the PDE6 δ subunit is present in the hypotonic extract ROS fraction and remains associated with the complex after gel-filtration (Figure 1(b), lanes 7 and 8, respectively). The δ subunit is probably sub-stoichiometric, since the hypotonic extract contains both soluble PDE6 complexes that contain δ and membrane-bound PDE6 complexes that are solubilized by the hypotonic treatment and are depleted in δ subunits. The gel-filtration step removed most contaminating protein bands present in the ROS fraction, and resulted in a purified PDE6 complex containing mainly the $\alpha\beta$ catalytic subunits.

Electron microscopy observation of the PDE6 complexes

Direct electron microscopy observation of the purified PDE6 molecules, adsorbed onto a carbon film and negatively stained with uranyl acetate, revealed mostly slightly elongated particles about $10 \text{ nm} \times 14 \text{ nm}$ in size (Figure 2(a)). A total of 1896 images corresponding to the major molecular population were extracted from the original micro-

graphs and analysed to describe in more detail the molecular organization of the PDE6 molecule.

Once brought to a common origin, the molecular images were analysed by multivariate statistical procedures and by classification methods to identify subsets of similar images. This analysis identified preferential molecular views with different in-plane orientations, which were used as references for rotational and translational alignment of the data set. Interestingly, the two first non-trivial eigenvectors, which are themselves images, showed a 2-fold symmetry and were rotated by 90° one with respect to the other. This symmetry of the eigenvectors reflects the symmetry properties of the structure and indicates that the complex contains two almost identical subunits related by a 2-fold symmetry (data not shown).²⁷ The aligned data set was clustered and the most representative class averages were used as new alignment references. The sequence of alignment and classification was iterated four times until the clustering into 50 classes was stable, and Figure 2(b) shows some characteristic class averages.

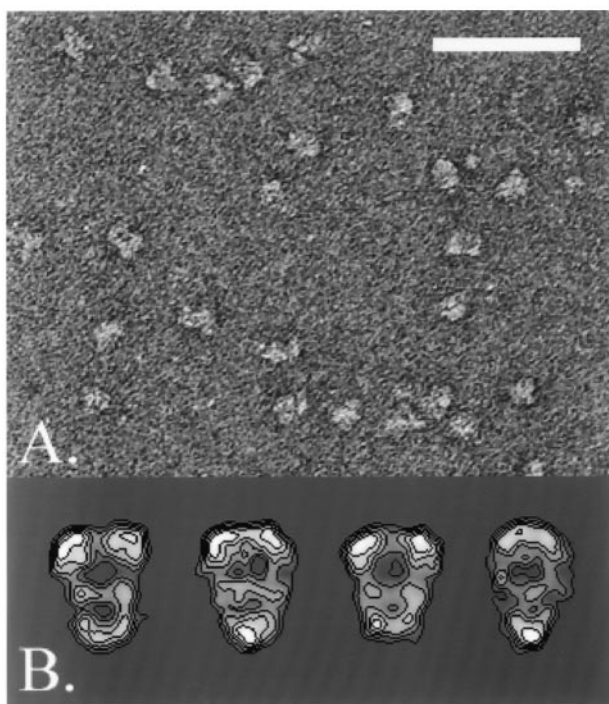


Figure 2. Electron microscopy observation and image analysis of PDE6 molecules purified from bovine rod outer segments. (a) Electron micrograph of PDE6 molecules adsorbed onto a carbon film and negatively stained with uranyl acetate showing the homogeneity in size and the dispersion of the complexes. (b) Gallery of the most representative PDE6 views obtained upon averaging aligned images clustered into homogeneous classes. The stain-excluding protein densities are represented in white and are outlined by contours of equal density. The four views correspond to different orientations of the molecule. The scale bar represents 58 nm in (a) and 16 nm in (b).

Some views show an almost perfect in-plane 2-fold symmetry axis, which confirm the symmetry properties of the eigenvectors and indicate that the particles are composed of two similar entities, referred to as asymmetric units. The other classes most probably correspond to the same molecular arrangement viewed through different orientations. Several views, corresponding to a majority of the original images, are clearly produced by a rotation around the symmetry axis. The particles are 11 nm \times 14 nm in size and show two stain-accessible holes within the dimer interface. Each is composed of three distinct domains forming a linear arrangement. The largest apical domain, about 4.5 nm in size, is connected through thin linkers to two smaller subdomains, about 3.5 nm in size each. The interface between the asymmetric units is formed by interactions between homologous sub-domains. The observed 2-fold symmetry is consistent with the biochemical data, indicating that PDE6 molecules are composed primarily of

two highly homologous $\alpha\beta$ subunits representing 85% of the mass of the complex.

Three-dimensional model of the PDE6 complexes

To investigate the 3D organization of the PDE6 molecules, a conical tilt series was recorded. A subset of molecular images corresponding to a unique PDE6 orientation were selected from the untilted image data set and a preliminary 3D model was reconstructed from the corresponding tilted images. This reconstruction was refined for translational misalignments and slight variations in projection direction, and was then used to determine the orientation of other PDE6 views revealed upon analysis of the untilted image data set by using sinogram correlation functions. Two additional alignment/reconstruction cycles were performed, after which the resulting 3D model was stable and the orientation plot shows that all possible orientations of the complex could be found in the untilted data set (Figure 3(a)). The resolution test

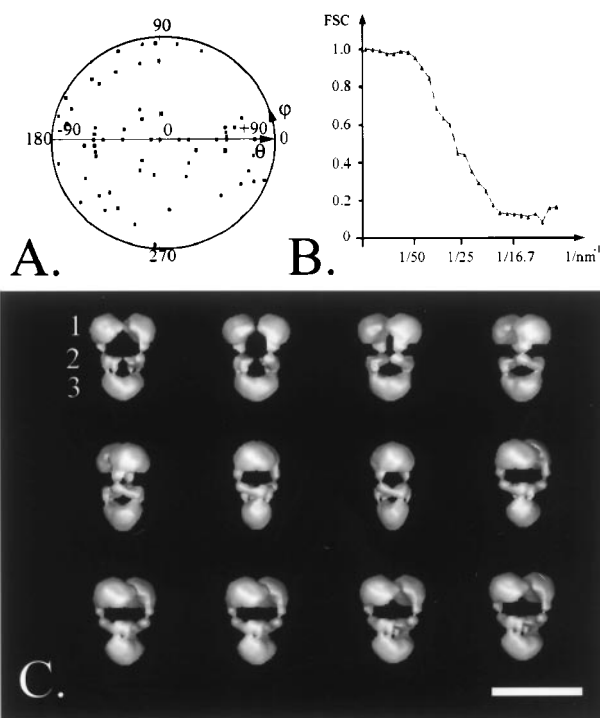


Figure 3. Three-dimensional model of bovine rod PDE6. (a) A diagram showing the orientations of the 64 class averages used in the final reconstruction. Each class-average is represented by a point in a (θ, ϕ) coordinate system. (b) Diagram representing the Fourier shell correlation function between two independent reconstructions. The vertical axis indicates the value of the Fourier shell correlation coefficient *versus* the resolution in 1/nm represented on the horizontal axis. (c) Surface representation of the 3D reconstruction of the bovine rod PDE6 at a resolution of 2.8 nm. The model is turned around a vertical axis by increments of 30°. The scale bar represents 15 nm.

performed on two independent data sets gave a value of 2.8 nm based on the 0.5 cut-off for the Fourier shell correlation coefficient (Figure 3(b)). The 2-fold symmetry was imposed because the asymmetric units could not be differentiated at the present resolution.

The PDE6 complex appears as a slightly elongated and flat particle 14.5 nm × 11.4 nm × 7.5 nm in size (Figure 3(c)). The density threshold corresponds to a volume of about 200 kDa (assuming a protein density of 1.4 g/cm³), consistent with the mass of PDE6 calculated from the amino acid sequences of the α and β subunits. Each asymmetric unit, 14.5 nm × 5.5 nm × 7.5 nm in size, consists of a linear arrangement of three subdomains connected by thin linkers. The largest domain (1) occupies a relative volume of 57% (corresponding to about 56 kDa). Domain 2 represents 15% (corresponding to about 15 kDa), whereas domain 3 occupies 28% of the volume (corresponding to about 27 kDa). The major contacts between the asymmetric units occur between the two homologous domains 3 and, to a lesser extent, between the domains 2, whereas the largest domains (1) do not interact.

Electron microscopy observation of PDE5 molecules

In order to confirm that this molecular arrangement is common to other phosphodiesterase families, human platelet PDE5 was purified and observed under the same conditions. The cytosolic fraction of human platelets was precipitated in ammonium sulphate. The solubilized fraction was separated by DEAE-Sepharose chromatography as described.²⁸ Fractions hydrolyzing cGMP and inhibited by the PDE5-specific inhibitor zaprinast were pooled and loaded onto an NH₂-zaprinast affinity column. Following elution with a 25 mM cGMP-containing buffer, the PDE was further purified by anion-exchange HPLC.²⁹ A single, symmetrical peak of cGMP hydrolytic activity was resolved (Figure 3(a)). This peak was analysed by SDS-PAGE (8% polyacrylamide) and a major band at a molecular mass of 85 kDa was detected by Coomassie blue staining (Figure 4(b), lane 1). Western blot analysis performed using a PDE5-specific antibody¹⁴ against native bovine lung PDE5³⁰ revealed two bands, at 85 kDa and 90 kDa (Figure 4(b), lane 2). The trypsin-digested bands were analysed by matrix-assisted laser desorption/ionization time-of-flight (MALDI-TOF) mass spectrometry (data not shown), which confirmed that the major band at 85 kDa corresponds to the PDE5 subunit, whereas the minor band at 90 kDa corresponds to a contaminant protein (glycogen phosphorylase). The faster migration of the PDE5 subunit was not investigated further but could be explained by specific post-translational modifications, limited proteolysis during purification or by the presence of a splicing variant of PDE5.³¹ The purified human platelet PDE5 had K_m

and V_{max} values of 0.27 μ M and 4.3 nmol min⁻¹ mg⁻¹, respectively. NH₂-zaprinast and DMPPPO were found to inhibit the purified enzyme with IC₅₀ values in the nanomolar range (data not shown).

In order to investigate the molecular organization of the PDE5 enzyme, the purified molecules were processed for electron microscopy as described above for the PDE6 complexes. A total of 1406 molecular images of PDE5 complexes were analysed similarly to the PDE6 data set. Although PDE5 contains a single isoform of the catalytic subunit,³⁰ a dimeric architecture was found for this enzyme also, consistent with biochemical evidence for a catalytic dimer.³² Since the views of the PDE5 and the PDE6 complexes appeared similar, the angular assignment of the PDE5 views could be performed by using the PDE6 model as a reference. The 3D models of the two enzymes were found to be similar (Figure 4(c)) both in the shape of the asymmetric units and in their dimeric interactions. Since both the PDE5 and the PDE6 monomer revealed three electron-dense subdomains, this common organisation reflects essentially the catalytic subunits and not the low molecular mass γ and δ subunits. This structural homology reflects the high level of sequence conservation between the catalytic subunits of PDE5 and PDE6, and underlines the conserved modular organisation of these proteins.

Immunolabelling of the N-terminal region of the PDE6 α subunit

Sequence alignment of the different cGMP-binding PDEs indicated that the highly homologous α and β subunits contain three major regions of sequence conservation corresponding to the C-terminal catalytic domain and to two regulatory GAF domains. The 3D model of the PDE6 molecule shows three structural domains, which may correspond to these three functional regions. To investigate this hypothesis, a polyclonal antibody raised against the N terminus of the bovine rod PDE6 α subunit (amino acid residues 1-10) was used to immunolabel the corresponding sequence on the PDE6 model. When the purified enzyme was incubated with a fivefold molar excess of antibody, labelled PDE6 molecules were clearly observed by electron microscopy (Figure 5(a)). To determine the interaction site of the antibody with the PDE6 complex, a total of 423 images of immune complex (IC) were recorded. Upon analysis, 296 IC images were found to correspond to the major orientation of the PDE6 molecules where the 2-fold symmetry axis lies in-plane. This subset of similarly oriented particles was analysed further to detect the specific location (e.g. most frequent occurrence) of an additional protein density arising from the binding of the antibody. Using this approach, a specific antibody-binding site could be determined at the tip of domain 3 (Figure 5(b)). This immunolabelling experiment showed that the

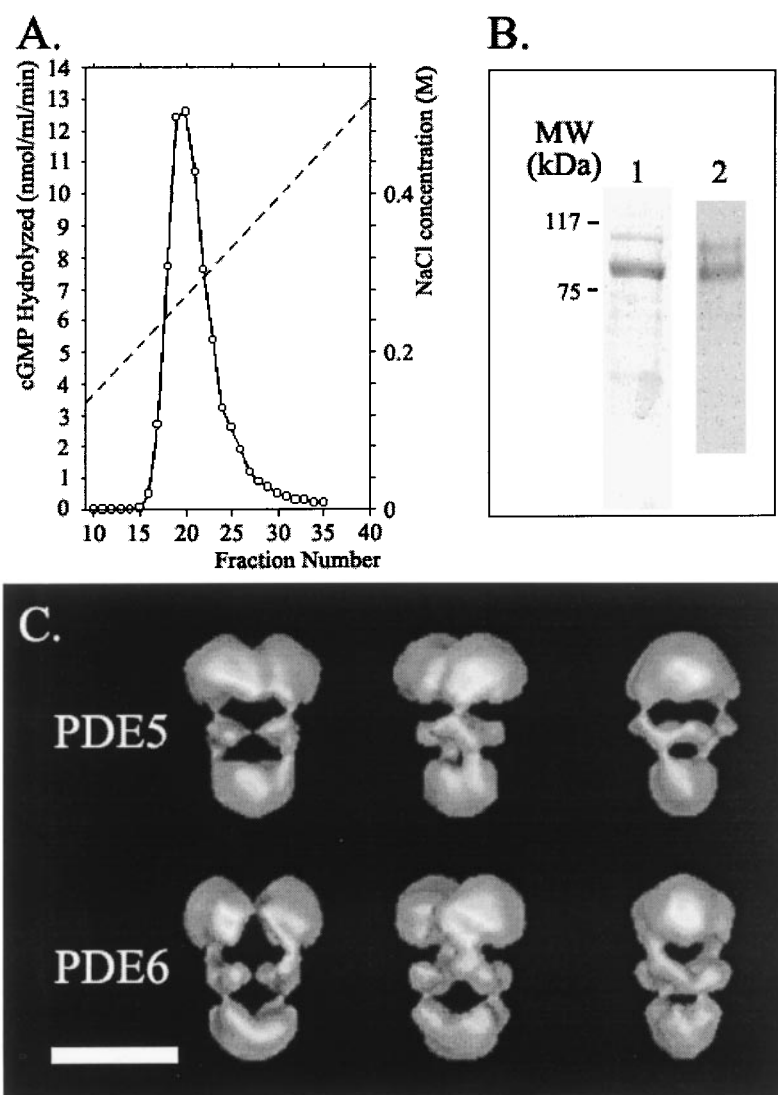


Figure 4. Structural comparison between purified human platelet PDE5 and bovine rod PDE6. (a) Activity profile of human platelet PDE5 purified on an ion-exchange HPLC column following a NH_2 -zaprinst affinity chromatography. Peak activity was observed at 0.25 M NaCl. (b) Protein analysis of the HPLC peak fraction described in (a): 50 ng of protein was analyzed by SDS-PAGE. Panel 1: the Coomassie stain reveals a major band at 85 kDa; Panel 2: The Western blot analysis using a lung PDE5-specific antibody,¹⁴ kindly provided by Dr J. D. Corbin, identifies the major band as PDE5. Molecular mass markers are indicated at the left of panel 1. (c) Surface representation of the 3D models of human platelet PDE5 and of bovine rod PDE6. The dimeric structure as well as the three-domain organization of each asymmetric unit are conserved in both enzyme forms. The models are turned around a vertical axis by increments of 45°. The scale bar represents 10 nm.

amino terminus of the α subunit is located at the end of the PDE6 molecule where the tightest interaction between the two monomers occurs, and suggests strongly that the C-terminal catalytic domains are located in the largest domain 1 (Figure 5(c)).

Discussion

In vertebrates, the large family of 3'-5' cyclic nucleotide phosphodiesterases is encoded by at least 21 genes, which have been subdivided into 11 groups according to their nucleotide sequences, kinetic behaviour, sensitivity to inhibitors and regulatory properties.^{11,12} Each PDE contains a conserved catalytic domain of about 275 amino acid residues in length placed near the carboxy-terminal ends of the protein. The amino-terminal parts of these proteins have regulatory functions, which differ between the PDEs and may involve calcium/calmodulin-binding sites, cGMP-binding sites, membrane localisation domains, and/or

phosphorylation sites. The family of PDEs containing GAF domains is composed of PDE2 (cGMP-stimulated), PDE5 (cGMP-binding), PDE6 (photo-receptor), PDE10 and PDE11. This group of PDEs contains allosteric cGMP-binding sites, which are distinct from the catalytic site and hold-specific functions. In PDE2, the binding of cGMP regulates the catalytic activity of the enzyme by increasing its affinity for cAMP.³³ In PDE5, the binding of cGMP increases the phosphorylation of the enzyme,³⁴ whereas cGMP binding to PDE6 strengthens the interaction between the PDE6-specific γ subunit and the catalytic subunits.^{13,35} The catalytic subunits of these enzymes can be organised into different oligomeric states. PDE2, PDE5 and cone PDE6 are believed to be functional as homodimers, whereas rod PDE6 forms a heterodimer of two distinct but highly homologous $\alpha\beta$ subunits. To date, only the PDE6 has been shown unequivocally to be associated with low molecular mass subunits that regulate the catalytic activity or the anchoring to the membrane.

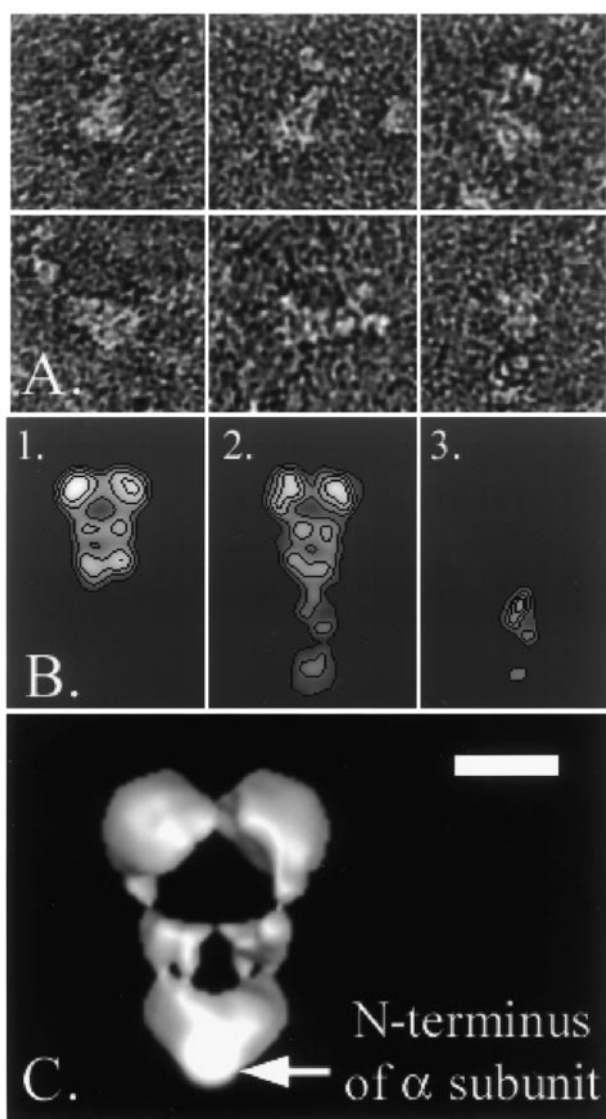


Figure 5. Immunolabelling of the N terminus of the PDE6- α subunit. (a) A gallery of PDE6 molecules labelled with an antibody specific for the N terminus of the α -subunit. (b) Panel 1 shows the class average of unlabelled molecules, whereas panel 2 represents the class average of labelled molecules. Panel 3 represents the difference map between the labelled and the unlabelled views. (c) The antibody-binding site is highlighted by an arrow on the surface representation of the 3D model of the PDE6 molecule. The scale bar represents 23 nm in (a), 10 nm in (b) and 5 nm in (c).

Direct electron microscopy observation of single molecules shows that the quaternary structure of two members of the cGMP-binding PDE family is highly similar. Purified human platelet PDE5 and bovine rod PDE6 are organized into a 2-fold symmetric arrangement, where each asymmetric unit has a modular organisation that can be subdivided into three individualised domains. This observation confirms previous biochemical evidence suggesting that PDE5 is organised into a homodi-

meric structure composed of two identical catalytic subunits.³² Since PDE5 does not associate with regulatory subunits, the modular three-domain architecture of the asymmetric unit must correspond to the molecular organisation of the catalytic subunits. The presently attained resolution of 2.8 nm is not sufficient to detect subtle differences between the catalytic α and β subunits of bovine rod PDE6. The dimer interface is traversed by solvent-accessible channels and the modular organisation into subdomains separated by solvent accessible channels provides a unique opportunity for the various effectors such as cGMP or the regulatory γ subunit to interact with their functional sites. The interactions between the catalytic subunits occur between homologous domains, and the specificity of these interfaces will determine the possible existence of $\alpha\alpha$ or $\beta\beta$ homodimers in the case of rod PDE6.³⁶ The major inter-subunits interaction are found to occur between the two domains 3 (Figure 3(c)), which we demonstrated by immunolabelling to correspond to the N terminus of the polypeptide. This observation is consistent with limited chymotryptic proteolysis, which localised the domain responsible for dimerisation to a 35 kDa N-terminal part of the PDE2 and PDE5 catalytic subunits.^{37,38}

The three-domain organisation observed for the human platelet PDE5 α subunit and the bovine rod PDE6 α and β subunits is likely to reflect the sequence conservation among the cGMP-binding PDEs. The two cGMP-binding domains (GAF domains) present in the N-terminal part of the sequence (repeats a and b) and the catalytic domain in the C-terminal end are likely to fold into independent units and to generate the observed modules. The GAF domains are predicted to fold into a globular structure similar to the crystal structure of the homologous yeast YKG9 protein,²¹ whereas the catalytic domain folds into a distinct domain that was shown to be functional independently of the GAF domains.^{20,32} Our immunolabelling experiment combined with the relative stain-exclusion volumes of each domain allows us to tentatively assign each domain relative to the primary sequence of the polypeptide. Domain 3 of PDE6 contains the N terminus, as indicated by our immunolabelling experiment, and its volume corresponds to approximately 27 kDa. This domain is likely to contain the cGMP-binding site referenced as repeat a.³⁹ Based on sequence alignment of several GAF domains,²¹ the length of repeat a was predicted to be of 184 residues (40-224) which, including the N terminus of the sequence, corresponds to a molecular mass of 25.5 kDa. The value is only slightly smaller than the relative volume of domain 3. Domain 2 is likely to hold the second cGMP-binding site (repeat b, from residues 225-433 of the PDE6 α subunit) and its calculated mass of 24.1 kDa is slightly larger but consistent with the relative volume of domain 2, which corresponds to 15 kDa. The sequence alignment predicts that

repeats a and b are almost identical in size, whereas the relative volumes in our model appear different. Interestingly, these alignments also show a small overlap between the two repeats, since the putative helix $\alpha 5$ of repeat a (residues 201-224) corresponds also to the predicted helices $\alpha 1$ and $\alpha 2$ of repeat b (residues 204-231). The different sizes of domains 2 and 3 thus suggests that the GAF domains have distinct folds, which may give a hint to the presence of two classes of cGMP-binding affinities.^{9,10,40} Finally, the size of domain 1 (relative volume of 56 kDa) is only slightly larger but consistent with the size of the catalytic domain (residues 434-858), which has a calculated mass of 49.7 kDa. Altogether these results suggest that the catalytic subunits of PDE5 and PDE6 are formed by three structural modules, organised linearly from the C terminus to the N terminus into a large catalytic domain and two smaller GAF domains.

Isoprenylation of the PDE6 catalytic subunits at their C terminus are responsible for anchoring the PDE molecule to the membrane.^{41,42} The linear organisation of the PDE6 molecule thus creates an oriented interaction with the membrane, where the catalytic domain is closest to the membrane and the regulatory cGMP-binding domains point towards the luminal side of the membrane. The δ subunit interacts with the prenylated C terminus of the catalytic domain and modulates the membrane anchoring of the PDE6 catalytic molecules.⁴³ The catalytic $\alpha\beta$ dimer is inhibited by the binding of the γ subunit to the catalytic pocket, and PDE6 activation during visual excitation results from the binding of the transducin T α subunit (itself tethered to the membrane by N-terminal myristylation) to the catalytic domain and the consequent displacement of PDE γ . The catalytic domain thus mediates interactions with various components of the visual signal transduction pathway.

It would have been of great interest to place the atomic structures of the catalytic domain determined from human recombinant PDE4B2B and of the consensus GAF domains into our 3D model. Unfortunately, the lack of structural details within our 3D model currently precludes a reasonable docking of our structures with the atomic coordinates. Additional experimental data, such as a mapping of the active site using a gold cluster, and/or labelling of the γ and δ subunit, will be need to provide a more detailed structure of the PDE6 catalytic subunits and their interactions with regulatory molecules.

Materials and Methods

Purification of bovine rod PDE6

Rod outer segments (ROS) were prepared essentially as described.⁴⁴ Briefly, retinas were dissected in dim red light from fresh bovine eyes, collected shortly after sacrifice and kept for two hours on solid CO₂. Retinas were suspended in buffer A (66 mM sodium phosphate (pH 7.0), 37% (w/v) sucrose), homogenized (potter), and

centrifuged (3000 g, 15 minutes). After diluting the supernatant with half a volume of buffer A without sucrose and centrifugation (25,000 g, 20 minutes), the pellet was submitted twice to a sucrose flotation by homogenisation in buffer A and horizontal centrifugation (45,000 g, 20 minutes). The red materials at the interface were washed three times with buffer A without sucrose (25,000 g, 20 minutes). The purified ROS were then suspended in buffer B (10 mM Tris-HCl (pH 7.4), 1 mM EDTA, 1 mM DTT) and centrifuged (100,000 g, 60 minutes).²² The resulting hypotonic extract contained a mixture of soluble PDE6, solubilized membrane-associated PDE6 and other components of the visual transduction signal. Highly purified PDE6 complexes were obtained by loading this hypotonic extract onto a Sephadex HR-200 gel-filtration column (Pharmacia) previously equilibrated with a buffer-containing 20 mM TrisHCl (pH 7.4), 150 mM NaCl, 1 mM DTT and eluted with the same buffer.

Purification of human platelet PDE5

Fresh human platelets were isolated from platelet-rich plasma kindly provided by the Centre de Transfusion Sanguine (CTS, Strasbourg, France). Blood plasma was centrifuged for ten minutes at 1200 g at room temperature in phosphate buffer A (187 mM NaCl, 2.7 mM KCl, 10 mM NaHPO₄-2H₂O, 1.8 mM KH₂PO₄, 5 mM glucose, pH 7.30). The resulting pellet was washed twice with buffer A and stored at -80°C. The sample was homogenised in ten volumes of platelet buffer B (20 mM Tris-HCl (pH 7.5), 2 mM magnesium acetate, 1 mM DTT, 1 mM EGTA) in the presence of a cocktail of proteases inhibitors. The homogenate was centrifuged for one hour at 105,000 g and the supernatant was precipitated overnight in 50% saturated (NH₄)₂SO₄. The precipitate was resuspended in platelet buffer B, dialysed overnight against buffer C (20 mM Tris-HCl (pH 7.4), 2 mM magnesium acetate, 1 mM EGTA). This fraction was loaded onto an anion-exchange chromatography column (2.4 cm × 15 cm, DEAE-Sepharose, Pharmacia) previously equilibrated with buffer B. The elution was performed with an NaCl gradient (0-0.5 M in buffer B) and 3 ml fractions were collected. PDE activity was assayed for 1 μ M cAMP or cGMP in the presence and in the absence of calcium/calmodulin (CaM).²⁸

Fractions with cGMP hydrolytic activities insensitive to calcium/calmodulin and inhibitable by zaprinast, were pooled and applied onto an affinity chromatography column composed of resin coupled with NH₂-zaprinast. After loading, the column was washed with buffer D (10 mM Tris-HCl, 500 mM NaCl) and the PDE5 was eluted with buffer D containing 25 mM cGMP and 2% (v/v) DMSO. The elution volume was dialysed overnight against buffer C and loaded onto an ion-exchange HPLC (Mono Q[®] HR5/5). The fractions containing the PDE5 activity were concentrated by centrifugation using Millipore filters (UFC4LTK25), and a final concentration of 25% (w/v) glycerol was added for storage at -20°C.

PDE activity assays

PDE activity was measured by a two-step radioenzymatic assay according to Keravis *et al.*⁴⁵ at a substrate concentration of 1 μ M cGMP in the presence of 14,000 cpm [³H]cGMP as a tracer. The total assay volume was 250 μ l containing 40 mM Tris-HCl (pH 7.5), 1 mM magnesium acetate, 1 mg/ml bovine serum albumin, 1 mM

EGTA. The enzyme was diluted so that <15% of the cGMP was hydrolysed. The product, which was isolated by anion-exchange chromatography (QAE Sephadex), was measured in a liquid scintillation counter. All drugs were dissolved in DMSO at a final concentration of 1%. The IC_{50} (concentration of the drug that inhibited 50% of the enzymatic activity) values were calculated by non-linear regression (Graphpad prism) and represented the mean of three determinations. K_m and V_{max} values were determined on a Lineweaver-Burk plot using cGMP ranging from 0.3 to 40 μ M.

PDs analysis by SDS-PAGE and immunodetection

Purified and concentrated PDE5 from human platelet and bovine rod PDE6 proteins were analysed by SDS-PAGE (8% polyacrylamide). Gels were Coomassie-stained or transferred to PVDF membranes for Western blot analysis. The antibody-antigen complexes were detected using goat anti-rabbit IgG conjugated to horseradish peroxidase (Bio Rad) and ECL reagent (Amersham Corp.). The immunoblots were then exposed using Kodak X-ray film.

Electron microscopy and image processing

Purified rod PDE6 and platelet PDE5 were diluted to a concentration of 20 μ g/ml in a buffer containing 20 mM Tris-HCl (pH 7.4), 150 mM NaCl, 2 mM DTT: 10 μ l of this preparation was placed on a 10 nm thick carbon film previously treated by a glow-discharge in air. After two minutes of adsorption, the grid was negatively stained with a 2% (w/v) uranyl acetate solution. The images were formed on a Philips CM120 transmission electron microscope operating at 100 kV with a LaB6 filament. Areas covered with individual molecules were recorded under low-dose condition (less than 20 electrons/ \AA^2) at a nominal magnification of 45,000 \times either on SO163 films (Kodak) or on a Slow Scan CCD camera (Gatan).

The micrographs were digitized at 18 μ m raster size resulting in a pixel spacing of 0.4 nm on the object. The image processing was performed using the IMAGIC software package (Image Science Software, Berlin, Germany).⁴⁶ For the 3D reconstruction from the conical tilt series, a total of 2336 pairs of 50° tilted and untilted molecular images, 128 \times 128 pixels in size, were extracted from the original micrographs by interactive selection based on size and non-connectivity criteria. The images of the untilted PDE6 molecules were iteratively aligned in translation and rotation, factorial correspondence analysis was used to represent the images in a 64-dimensional factor space, and hierarchic ascendant classification schemes were used to cluster the images into classes of images with maximal resemblance.⁴⁷ In order to identify the first alignment references without bias, a reference-free method was used that consists of clustering the original data set once brought to a common origin.²⁷ Several alignment and classification cycles identified a major orientation of the particles and the corresponding tilted images, which constitute a conical tilt series, were combined to calculate a 3D model by weighted back-projection.⁴⁸ The resulting model was re-projected along the input directions in order to correct each original image for in-plane transitional misalignments and slight variations in euler angle assignment. This preliminary model was then re-projected along 105 equally spaced viewing directions to generate references

to align the untilted images. The aligned images were clustered into 100 classes and the angular assignment of each class average was performed using sinogram correlation functions against re-projections of the preliminary model. The 3D model was stable after two additional alignment/clustering cycles. The absolute hand of the structure is determined by the conical tilt approach and the different steps of the 3D reconstruction protocol were validated by comparing an electron microscopy-determined structure of RNA polymerase I with that of the atomic structure of the related RNA polymerase II determined by X-ray crystallography.

The resolution of the final reconstruction was estimated by the Fourier shell correlation function obtained by comparing two independent reconstructions generated by splitting the data set in half randomly. The two data sets were aligned and clustered independently and the resolution criterion was the 0.5 Fourier shell correlation cut-off.

The untilted PDE5 data set was analysed independently as described for the PDE6 data set in order to obtain representative class averages. The first angular assignment of these class averages was performed using sinogram correlation functions against re-projections of the PDE6 model. A first PDE5 model was calculated and was re-projected along uniformly distributed projection directions to generate new alignment references for the PDE5 data set. The aligned data set was clustered and the class averages were used to generate a new model. This alignment/clustering/reconstruction cycle was iterated twice up to the point where the 3D model was stable.

Immuno-electron microscopy

The antibody α -NT59 is directed against the N-terminal region of bovine rod PDE6 α subunit and was produced by injecting the peptide GEVTAEVEK (corresponding to amino acid residues 1-10 of bovine α subunit with an added Cys residue) into rabbits. The antibody was affinity-purified on a peptide-coupled column and showed an IC_{50} of 2×10^4 with 25 ng of PDE6 in ELISA tests. For immuno-electron microscopy, a three- to fivefold molar excess of antibodies was incubated for one hour at 20°C with purified PDE6 at a final protein concentration of 20 μ g/ml. The relative amounts of PDE6 and of antibodies were adjusted by electron microscopy inspection of the incubation mixture. The putatively labelled PDE6 molecules were identified by a stain-excluding domain protruding out of the molecule, whose size and shape were consistent with those of an IgG molecule. Images of such complexes were aligned and analysed as described.⁴⁹

Acknowledgements

We are grateful to Dr J. D. Corbin (Vanderbilt University, Nashville, USA) for the kind gift of lung PDE5 antibodies, to Drs J.M. Strub and A. Van Dorsselaer for MALDI-TOF mass spectrometry analysis, and to Drs J. P. Cazenave and C. Vallere (Centre de Transfusion Sanguine, Strasbourg, France) for providing us with human blood platelets. We thank M. Schatz for helpful advice with the IMAGIC software (Image Science Software, Berlin, Germany) and for customising the package. This work was supported by the Institut National de la Santé

et de la Recherche Médicale, the Centre National pour la Recherche Scientifique, the Hôpital Universitaire de Strasbourg (HUS), the Association pour la Recherche sur le Cancer, the Ligue contre le cancer, and the National Institutes of Health (EY 05798).

References

- Ovchinnikov, Y., Gubanov, V. V., Khramtsov, N. V., Ischenko, K. A., Zagranichny, V. E. & Muradov, K. G. *et al.* (1987). Cyclic GMP phosphodiesterase from bovine retina. Amino acid sequence of the alpha-subunit and nucleotide sequence of the corresponding cDNA. *FEBS Letters*, **223**, 169-173.
- Lipkin, V. M., Khramtsov, N. V., Vasilevskaya, I. A., Atabekova, N. V., Muradov, K. G. & Gubanov, V. V. *et al.* (1990). Beta-subunit of bovine rod photoreceptor cGMP phosphodiesterase. Comparison with the phosphodiesterase family. *J. Biol. Chem.* **265**, 12955-12959.
- Ovchinnikov, Y., Lipkin, V. M., Kumarev, V. P., Gubanov, V. V., Khramtsov, N. V. & Akhmedov, N. B. *et al.* (1986). Cyclic GMP phosphodiesterase from cattle retina. Amino acid sequence of the gamma-subunit and nucleotide sequence of the corresponding cDNA. *FEBS Letters*, **204**, 288-292.
- Deterre, P., Bigay, J., Forquet, F., Robert, M. & Chabre, M. (1988). cGMP phosphodiesterase of retinal rods is regulated by two inhibitory subunits. *Proc. Natl Acad. Sci. USA*, **85**, 2424-2428.
- Gillespie, P. G., Prusti, R. K., Apel, E. D. & Beavo, J. A. (1989). A soluble form of bovine rod photoreceptor phosphodiesterase has a novel 15-kDa subunit. *J. Biol. Chem.* **264**, 12187-12193.
- Florio, S. K., Prusti, R. K. & Beavo, J. A. (1996). Solubilization of membrane-bound rod phosphodiesterase by the rod phosphodiesterase recombinant delta subunit. *J. Biol. Chem.* **271**, 24036-24047.
- Pugh, E. N., Jr & Lamb, T. D. (2000). Phototransduction in vertebrate rods and cones: molecular mechanisms of amplification, recovery and light adaptation. In *Molecular Mechanisms in Visual Transduction*, (Stavenga, D. G. & Pugh, E. N., Jr, eds) pp. 183-255, Elsevier Science, New York.
- Aravind, L. & Ponting, C. P. (1997). The GAF domain: an evolutionary link between diverse phototransducing proteins. *Trends Biochem. Sci.* **22**, 458-459.
- Yamazaki, A., Sen, I., Bitensky, M. W., Casnellie, J. E. & Greengard, P. (1980). Cyclic GMP-specific, high affinity, noncatalytic binding sites on light-activated phosphodiesterase. *J. Biol. Chem.* **255**, 11619-11624.
- Norton, A. W., D'Amours, M. R., Grazio, H. J., Hebert, T. L. & Cote, R. H. (2000). Mechanism of transducin activation of frog rod photoreceptor phosphodiesterase: allosteric interactions between the inhibitory {gamma} subunit and the noncatalytic cGMP binding sites. *J. Biol. Chem.* **275**, 38611-38619.
- Conti, M. (2000). Phosphodiesterases and cyclic nucleotide signaling in endocrine cells. *Mol. Endocrinol.* **14**, 1317-1327.
- Francis, S. H., Turko, I. V. & Corbin, J. D. (2000). Cyclic nucleotide phosphodiesterases: relating structure and function. In *Prog. Nucl. Acid Res. Mol. Biol.*, vol. 65, pp. 1-52, .
- Artemyev, N. O., Arshavsky, V. Y. & Cote, R. H. (1998). Photoreceptor phosphodiesterase: interaction of inhibitory gamma subunit and cyclic GMP with specific binding sites on catalytic subunits. *Methods*, **14**, 93-104.
- McAllister-Lucas, L. M., Sonnenburg, W. K., Kadlecsek, A., Seger, D., Trong, H. L. & Colbran, J. L. *et al.* (1993). The structure of a bovine lung cGMP-binding, cGMP-specific phosphodiesterase deduced from a cDNA clone. *J. Biol. Chem.* **268**, 22863-22873.
- Gillespie, P. G. & Beavo, J. A. (1989). Inhibition and stimulation of photoreceptor phosphodiesterases by dipyrindamole and M&B 22,948. *Mol. Pharmacol.* **36**, 773-781.
- D'Amours, M. R., Granovsky, A. E., Artemyev, N. O. & Cote, R. H. (1999). Potency and mechanism of action of E4021, a type 5 phosphodiesterase isozyme-selective inhibitor, on the photoreceptor phosphodiesterase depend on the state of activation of the enzyme. *Mol. Pharmacol.* **55**, 508-514.
- Tate, R. J., Lochhead, A., Brzeski, H., Arshavsky, V. & Pyne, N. J. (1998). The gamma-subunit of the rod photoreceptor cGMP-binding cGMP-specific PDE is expressed in mouse lung. *Cell Biochem. Biophys.* **29**, 133-144.
- Lochhead, A., Nekrasova, E., Arshavsky, V. Y. & Pyne, N. J. (1997). The regulation of the cGMP-binding cGMP phosphodiesterase by proteins that are immunologically related to gamma subunit of the photoreceptor cGMP phosphodiesterase. *J. Biol. Chem.* **272**, 18397-18403.
- Corbin, J. D. & Francis, S. H. (1999). Cyclic GMP phosphodiesterase-5: target of sildenafil. *J. Biol. Chem.* **274**, 13729-13732.
- Xu, R. X., Hassell, A. M., Vanderwall, D., Lambert, M. H., Holmes, W. D. & Luther, M. A. *et al.* (2000). Atomic structure of PDE4: insights into phosphodiesterase mechanism and specificity. *Science*, **288**, 1822-1825.
- Ho, Y. S., Burden, L. M. & Hurley, J. H. (2000). Structure of the GAF domain, a ubiquitous signaling motif and a new class of cyclic GMP receptor. *EMBO J.* **19**, 5288-5299.
- Pellicone, C., Cook, N. J., Nullans, G. & Virmaux, N. (1985). Light-induced conformational change in rhodopsin detected by modification of G-protein binding, GTP gamma S binding and cGMP phosphodiesterase activation. *FEBS Letters*, **181**, 184-188.
- Estrade, M., Grondin, P., Cluzel, J., Bonhomme, B. & Doly, M. (1998). Effect of a cGMP-specific phosphodiesterase inhibitor on retinal function. *Eur. J. Pharmacol.* **352**, 157-163.
- Coste, H. & Grondin, P. (1995). Characterization of a novel potent and specific inhibitor of type V phosphodiesterase. *Biochem. Pharmacol.* **50**, 1577-1585.
- Deterre, P., Bigay, J., Robert, M., Pfister, C., Kuhn, H. & Chabre, M. (1986). Activation of retinal rod cyclic GMP-phosphodiesterase by transducin: characterization of the complex formed by phosphodiesterase inhibitor and transducin alpha-subunit. *Proteins: Struct. Funct. Genet.* **1**, 188-193.
- Deterre, P., Bigay, J., Forquet, F., Robert, M. & Chabre, M. (1988). cGMP phosphodiesterase of retinal rods is regulated by two inhibitory subunits. *Proc. Natl Acad. Sci. USA*, **85**, 2424-2428.
- Dube, P., Tavares, P., Lurz, R. & van Heel, M. (1993). The portal protein of bacteriophage SPP1: a DNA pump with 13-fold symmetry. *EMBO J.* **12**, 1303-1309.
- Lugnier, C., Schoeffter, P., Le Bec, A., Strouthou, E. & Stoclet, J. C. (1986). Selective inhibition of cyclic

- nucleotide phosphodiesterases of human, bovine and rat aorta. *Biochem. Pharmacol.* **35**, 1743-1751.
29. Lugnier, C., Muller, B., Le Bec, A., Beaudry, C. & Rousseau, E. (1993). Characterization of indolidan- and rolipran sensitive cyclic nucleotide phosphodiesterases in the canine and human cardiac microsomal fractions. *J. Pharmacol. Exp. Ther.* **265**, 1142-1151.
 30. Thomas, M. K., Francis, S. H. & Corbin, J. D. (1990). Characterization of a purified bovine lung cGMP-binding cGMP phosphodiesterase. *J. Biol. Chem.* **265**, 14964-14970.
 31. Lin, C. S., Lau, A., Tu, R. & Lue, T. F. (2000). Expression of three isoforms of cGMP-binding cGMP-specific phosphodiesterase (PDE5) in human penile cavernosum. *Biochem. Biophys. Res. Commun.* **268**, 628-635.
 32. Fink, T. L., Francis, S. H., Beasley, A., Grimes, K. A. & Corbin, J. D. (1999). Expression of an active, monomeric catalytic domain of the cGMP-binding cGMP-specific phosphodiesterase (PDE5). *J. Biol. Chem.* **274**, 34613-34620.
 33. Murashima, S., Tanaka, T., Hockman, S. & Manganiello, V. (1990). Characterization of particulate cyclic nucleotide phosphodiesterases from bovine brain: purification of a distinct cGMP-stimulated isoenzyme. *Biochemistry*, **29**, 5285-5292.
 34. Corbin, J. D., Turko, I. V., Beasley, A. & Francis, S. H. (2000). Phosphorylation of phosphodiesterase-5 by cyclic nucleotide-dependent protein kinase alters its catalytic and allosteric cGMP-binding activities. *Eur. J. Biochem.* **267**, 2760-2767.
 35. Yamazaki, A., Bondarenko, V. A., Dua, S., Yamazaki, M., Usukura, J. & Hayashi, F. (1996). Possible stimulation of retinal rod recovery to dark state by cGMP release from a cGMP phosphodiesterase noncatalytic site. *J. Biol. Chem.* **271**, 32495-32498.
 36. Artemyev, N. O., Surendran, R., Lee, J. C. & Hamm, H. E. (1996). Subunit structure of rod cGMP-phosphodiesterase. *J. Biol. Chem.* **271**, 25382-25388.
 37. Thomas, M. K., Francis, S. H. & Corbin, J. D. (1990). Substrate- and kinase-directed regulation of phosphorylation of a cGMP-binding phosphodiesterase by cGMP. *J. Biol. Chem.* **265**, 14971-14978.
 38. Stroop, S. D. & Beavo, J. A. (1991). Structure and function studies of the cGMP-stimulated phosphodiesterase. *J. Biol. Chem.* **266**, 23802-23809.
 39. Trong, H. L., Beier, N., Sonnenburg, W. K., Stroop, S. D., Walsh, K. A., Beavo, J. A. & Charbonneau, H. (1990). Amino acid sequence of the cyclic GMP stimulated cyclic nucleotide phosphodiesterase from bovine heart. *Biochemistry*, **29**, 10280-10288.
 40. Mou, H., Grazio, H. J. III, Cook, T. A., Beavo, J. A. & Cote, R. H. (1999). cGMP binding to noncatalytic sites on mammalian rod photoreceptor phosphodiesterase is regulated by binding of its gamma and delta subunits. *J. Biol. Chem.* **274**, 18813-18820.
 41. Ong, O. C., Ota, I. M., Clarke, S. & Fung, B. K. (1989). The membrane binding domain of rod cGMP phosphodiesterase is posttranslationally modified by methyl esterification at a C-terminal cysteine. *Proc. Natl Acad. Sci. USA*, **86**, 9238-9242.
 42. Catty, P. & Deterre, P. (1991). Activation and solubilization of the retinal cGMP-specific phosphodiesterase by limited proteolysis. Role of the C-terminal domain of the beta-subunit. *Eur. J. Biochem.* **199**, 263-269.
 43. Cook, T. A., Ghomashchi, F., Gelb, M. H., Florio, S. K. & Beavo, J. A. (2000). Binding of the delta subunit to rod phosphodiesterase catalytic subunits requires methylated, prenylated C termini of the catalytic subunits. *Biochemistry*, **39**, 13516-13523.
 44. Virmaux, N., Urban, P. F. & Wachneldt, V. T. (1971). Proteins of bovine retinal outer segments electrophoresis on polyacrylamide gels in the presence of sodium dodecyl sulfate. *FEBS Letters*, **12**, 325-328.
 45. Keravis, T. M., Wells, J. N. & Hardman, J. G. (1980). Cyclic nucleotide phosphodiesterase activities from pig coronary arteries. Lack of interconvertibility of major forms. *Biochim. Biophys. Acta*, **613**, 116-129.
 46. van Heel, M., Harauz, G. & Orlova, E. V. (1996). A new generation of the IMAGIC image processing system. *J. Struct. Biol.* **116**, 17-24.
 47. van Heel, M. & Frank, J. (1981). Use of multivariate statistics in analysing the images of biological macromolecules. *Ultramicroscopy*, **6**, 187-194.
 48. Radermacher, M., Wagenknecht, T., Verschoor, A. & Frank, J. (1986). A new 3-D reconstruction scheme applied to the 50S ribosomal subunit of *E. coli*. *J. Microsc.* **141**, RP1-RP2.
 49. Schultz, P., Fribourg, S., Poterszman, A., Mallouh, V., Moras, D. & Egly, J. M. (2000). Molecular structure of human TFIIF. *Cell*, **102**, 599-607.

Edited by W. Baumeister

(Received 10 January 2001; received in revised form 23 May 2001; accepted 29 May 2001)